ChemComm

Accepted Manuscript

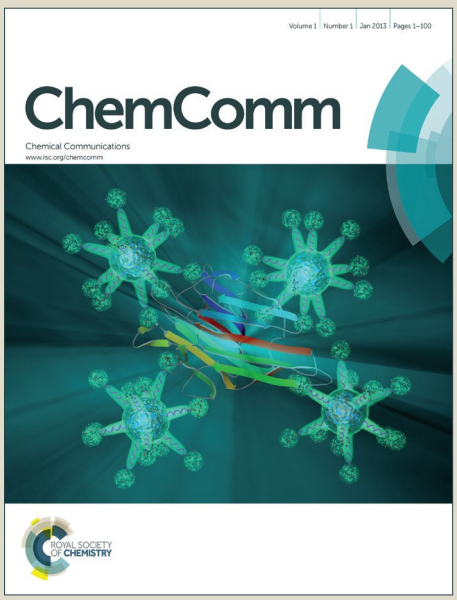

ROYAL SOCIETY OF CHEMISTRY

www.rsc.org/chemcomm

ChemComm

COMMUNICATION

Metal-Organic Frameworks derived Hollow polyhedron Metal Oxide Posited Graphene oxide for Energy Storage Applications

Received 00th January 20xx,
Accepted 00th January 20xx

DOI: 10.1039/x0xx00000x

www.rsc.org/

Bendi Ramaraju*, Cheng-Hung Li, Sengodu Prakash and Chia-Chun Chen*

A composite made from hollow polyhedron copper oxide and graphene oxide was synthesized by sintering a Cu-based metal–organic framework (Cu-MOF) embedded with exfoliated graphene oxide. As a proof-of-concept application, the obtained Cu_{ox}-rGO materials were used in a lithium-ion battery and sodium-ion battery as an anode material. Overall, Cu_{ox}-rGO composite delivers excelent electrochemical properties with stable cycling when compared to pure CuO-rGO and Cu-MOF.

The energy issue is one of the very hot topics in the society due to the development of the economy, which requires cost-effective, efficient and environmentally benign energy storage devices that can empower energy demanding areas. Owing to their high energy density, light weight and long cycle lives, rechargeable batteries (RBs) have shown considerable promise for storage devices.[1-2] The successful utilization of RBs depends strongly on the preparation of nanomaterials with outstanding storage properties. Recent progress has demonstrated that nanostructured transition metal oxides are very attractive candidates for RBs anodes due to their high storage capacities.[3-5]

Metal–organic frameworks (MOF) are a novel class of porous materials, which has attracted considerable interest due to their potential applications in catalysis, nonlinear optics, ion exchange, gas storage and separation.[6–10] Among the various forms of carbonaceous materials, graphene and graphene-based materials are on the top notch, owing to their specific and very unique structural, mechanical, and electronic properties of these one-atom-thick sheets.[11,12] Graphite oxide (GO) is formed by treating graphite with very strong oxidizing agents[13]. Oxidation of graphite results in the introduction of epoxy and hydroxyl groups into the graphene layers and carboxylic acid groups mainly located at the edges of the layers.[14,15]

Department of Chemistry, National Taiwan Normal University, Taipei 116, Taiwan. E-mail: ramarajubendi@gmail.com; cjchen@ntnu.edu.tw
Electronic Supplementary Information (ESI) available: [details of any supplementary information available should be included here]. See DOI: 10.1039/x0xx00000x

Recently, the hybrids of MOFs and graphene derivatives have attracted significant attention because of its good structural scaffold as it stabilizes the physical structure during charge-induced volume expansion, which further improved the conductivity of metal oxides. Graphene has a wide scope to act as an ideal conducting additive for hybrid composite electrodes.[16-26] Furthermore, when the GO was reduced to reduced graphene oxide (rGO), it can overcome the poor electrical conductivity of the MOF; thus, MOF/rGO composites can be used as promising electrode materials for electrocatalysis.[27] To date, there are only few reports on GO–CuO composites prepared by chemical methods.[28–33] Herein, we report a simple synthetic strategy to prepare Cu_{ox}-rGO (CuO/Cu_2O hollow polyhedrons on rGO). Further the applications such as, lithium-ion batteries (LIBs) and sodium-ion batteries (NIBs) were demonstrated.

Morphology of the Cu-MOF and Cu_{ox}-rGOwere shown in ESI† (Fig S4-S9). Cyclic voltammetry (CV) was employed to study the reaction mechanism during electrochemical cycling in half-cell assembly (Li/ Cu_{ox}-rGO) between 0.005–3 V vs. Li at a slow scan rate of 0.1 mV s^{-1} (see Figure 1A). During first cathodic scan, a prominent peak at ~1.08 V is noted, which is attributed to the formation of the Cu_2O phases and associated structural destruction as well. Another small cathodic peak at ~0.69 V corresponds to the further reduction of CuO to metallic Cu^o in Li_2O matrix, though decomposition of the electrolyte solution cannot be ruled out. Decomposition of the electrolyte solution leads to the formation of polymeric layers and inorganic byproducts in the form of solid electrolyte interface (SEI). During anodic scan, the peak at ~2.45 V corresponds to the oxidation of Cu^o to CuO as well.[34-37]From 2nd cycle onwards, cathodic peak potentials were slightly shifted towards higher voltages, whereas no significant shift in the peak positions is noted during anodic scan. Accordingly, the reduction of CuO to Cu_2O occurs at ~1.3 V and formation of metallic Cu^o takes place at ~0.84 V with huge suppression of area underneath the curve when compared to the first cathodic sweep.[35] However, there is no deviation observed during successive cycles except overlapping of the traces

which implies good cycleability of the CuO nanostructures during cycling. The formation of intermediate phase (Cu_2O) has been convincingly proven by Tarascon and co-workers[34,36] by ex-situ TEM analysis and Wei et al. by CV studies.[37] Therefore, the conversion reaction can be written as

Cathodic scan

$$2CuO + 4Li^+ + 4e^- \xrightarrow{\text{lithiation}} Cu_2O \xrightarrow{\text{lithiation}} 2Cu^0 + 2Li_2O$$

Anodic scan

$$Cu^0 + Li_2O \xrightarrow{\text{delithiation}} CuO + 2Li^+$$

At subsequent charge-discharge cycle

$$CuO + 2Li^+ + 2e^- \leftrightarrow Cu^0 + Li_2O$$

Galvanostatic charge - discharge studies were conducted for Cu_{ox}-rGO nanostructures in half-cell assembly (Li/Cu_{ox}-rGO) at a constant current density of 200 mA g^{-1} and the data are shown in Fig. 1B. In the figure there are two obvious sloping potential ranges (1.35–1.0 and 1.0–0.05 V vs Li^+/Li, respectively) in the first discharge process, which are in accordance with the two cathodic peaks in the CVs in Fig. 1A. During the following discharge process, all the slopes become narrow and the plateau slightly upward. Upon the charging process, a plateau at about 2.45 V can be clearly identified during all the charge cycles was recorded. The half-cell delivered the capacity of ~1324 and ~690 mAh g^{-1} for first discharge and charge, respectively. This can be attributed to large electrochemical active surface of well-dispersed graphene and to the large area of SEI in the well dispersed Cu_{ox}. As expected, huge irreversible capacity of 52.1% is noted in the first cycle, the initial capacity loss is mainly resulted from diverse irreversible process, such as interfacial lithium storage, inevitable formation of SEI layer, organic conductive polymer, and electrolyte decomposition, which are common for most anode materials.[34,35,38-42]

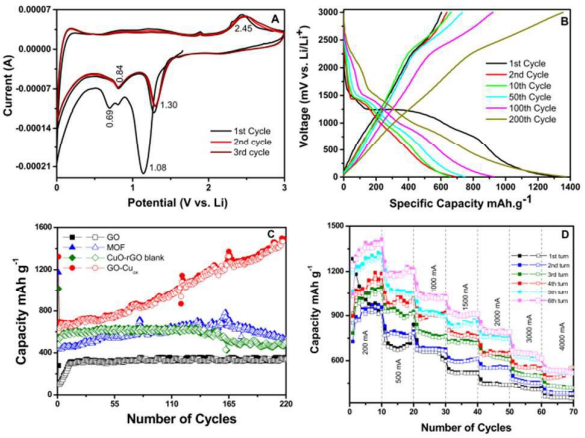

Figure 1. Lithium-ion-battery performance: A) cyclic voltammograms of Cu_{ox}-rGO composite electrode at a scan rate of 0.1 mV s^{-1} between 0–3.0 V, B) Discharge–charge curves of ofCu_{ox}-rGO composite electrode between 0.05–3.0 V at 200 mA. g^{-1} current rate, C) cycle performance various electrodes at 200 mA. g^{-1} current rate, D) cycle performance of Cu_{ox}-rGO composite electrode at different current rate.

Fig. 1C shows the cycling performance of different electrodes (GO, MOF, CuO-rGO blank and Cu_{ox}-rGO) at a current density of 200 mA g^{-1}. It can be seen that, when compared with other samples, the electrode with Cu_{ox}-rGO exhibits the best electrochemical performance with a reversible capacity of about 1490 mAh g^{-1} after 220 cycles. It is remarkably noticed that the capacity decreases first and reaches a minimum (650 mAh g^{-1}) at 3rd cycle. It rises gradually afterwards and reaches about 1490 mAh g^{-1} at 220th cycle. It can be seen that the capacity of Cu_{ox}-rGO recovers after initial fading for the first few cycles. The slow increase in the specific capacity during cycling has also been reported on metal-oxide electrodes.[43] In this case, the capacity increases by a significant amount to 1490 mAh g^{-1} at 220th cycle. This increase in the capacity might be a result of electrochemical exfoliation of graphene sheets, which seems to be more at higher current rate and capable of bringing extra Li into active traverse between electrodes. Exfoliation of graphene sheets is proven to create additional room (availability of active surface area) for increased Li adsorption onto their surfaces.[44] This kind of increase in the capacity due to volumetric changes caused by exfoliation of graphene sheets was observed in the case of carbon nanofibers[44] upon long-term cycling, but in the case of Cu_{ox}-rGO, it is observed at a much early stage of aging. Here the surfaces of Cu_{ox} nanoparticles, which are expected to possess highly catalytic nature, and are expected to avoid Li dendrite formation by decreasing the repulsive interactions between Li - Li ions like electron-deficient dopants do in the case of modified graphene.[45] Thus, Cu_{ox} nanoparticles also reasonably support the long-time sustainability of anode functioning without failure yet with increased capacity. Recent report of MgO-decorated few-layered graphene by Shaikshavali et al. was supports this explanation.[46] In the meanwhile, the Cu_{ox}-rGO electrode exhibits outstanding rate capability at different current densities of 200-4000 mA g^{-1} (Fig 1D). The cell also shows good capacity retention even after changing back the current density of 200 mA g^{-1}. Moreover, the prominent structural advantage of Cu_{ox}-rGO enables substantially improved cycle life at a high current rate (1000 mA g^{-1}); Cu_{ox}-rGO still exhibited ~1100 mA g^{-1} after 600 cycles (Fig. 3a). These results imply that the electrode structure of Cu_{ox}-rGO allowing it to exhibit stable cycle performance at a high rate over 600 cycles without capacity fading. Overall It was clear cut that Cu_{ox}-rGO composite possesses excellent properties such as high rate capability, good cycling performance, and a capacity that increases upon cycling, which are very useful for high-power battery applications, such as in hybrid electric vehicles, power tools, and power backup systems.

The benefit of using Cu_{ox}-rGOas an anode material in battery become evident, when the electrochemical impedance spectroscopy (EIS) was performed as shown in Figure 2. Figure 2A represents Nyquist plot of Cu_{ox}-rGO along with the other electrode systems. Nyquist plot shows the existence of both kinetics and diffusion components. In which two distinct semicircles were observed in the high- and middle-frequency regions, which could be attributed to the resistance of the SEI and charge transfer resistance, respectively. Whereas, a straight line in the low-frequency region can be assigned to the diffusion resistance. The distortion in the peak shape could be due to the distribution in the SEI. The diameter of two semicircles is related to the two different time constants, which indicates Cu_{ox}-rGO not only possesses low SEI resistance (~114 ohm) but also very low charge transfer resistance (~166

ohm) in comparison with rest of the materials (Figure 2A and Table S1(ESI†)). This significant reduction in the charge transfer resistance stem from GO and Cu_{ox}, in which GO provides better electrode to electrolyte contact while Cu_{ox} provides a facile path for the conduction of the charge carriers. In the very low frequency region, a straight line in case of Cu_{ox}-rGO renders the information about the good capacitive behavior of the electrode material. The modeling of EIS spectra for MOF and Cu_{ox}-rGO electrodes' surface was done using Randles electrical equivalent circuit (Fig S10 (ESI†)). The results from the fit are presented in Table S1 (ESI†).

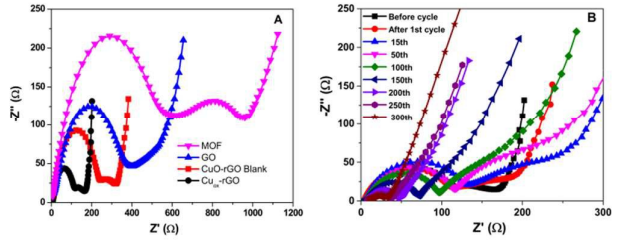

Figure 2. Lithium-ion-battery performance: A) Electrochemical impedance spectra of various electrodes B) Electrochemical impedance spectras of Cu_{ox}-rGO before cyclic performance and after 1st, 15th, 50, 100, 150, 200, 250 and 300th cycles.

In order to investigate the change in the EIS spectra of Cu_{ox}-rGO electrode, EIS spectrums of the electrode before and after 1st cycle, 15th cycle, and 50th cycle, and so on were collected upto 300 cycles, and represented in Figure 2B. It is evident from the EIS analyses that the charge resistance of the electrode increases with the cycling, which is reflected by the disappearance of the peak in the low frequency region. When the resistance for the intercalation reaction tends to infinite, the only reaction which could presumably occurs at the interface of electrode/electrolyte is adsorption of the ions, which is evident by the straight line in the low frequency region after 300th cycles.

It is also interesting to note that the capacity of the Cu_{ox}-rGO electrode shows two major trends. For the first few cycles, the capacity shows a decreasing trend, while for the next cycles, the capacity trend is increasing. The initial decrease may be due to the extraction of Li from Li_2O thermodynamically impossible, which has formed during the transformation of Cu^0 to Cu^{2+} or the irreversible reaction from Cu^0 to Cu^{2+}.[47] Electrochemical impedance spectroscopy (EIS) analysis was performed on the samples charge/discharge tests in order to obtain the charge-transfer resistance and investigate the kinetic behavior of the samples. The results revealed that the decrease in capacity upon cycling was may be due to two factors, namely, low lithium-diffusion processes and large Li^+ charge-transfer resistance (high polarization), which is also in good agreement with our study which states the impedance of the cell before cycling is smaller than that of the cell after cycling (Fig. 2B).

On the other hand, the trend towards increasing capacity could be at least partly explained by the following reasons: (1) decreased cell resistance, (2) the effects of electrochemical milling, which can change the morphology of a material and reduce the particle size. The first reason may relate to the decrease in the cell resistance during the charge/discharge reaction, as shown in Fig. 2B. In the figure, the impedance of the cell before cycling is larger than that of the cell after 15th cycling, and it becomes smaller after further charge–discharge up to 300 cycles, which is in good agreement with the capacity rise phenomena seen in CuO material.[48] This could be explained as follows: The initial production of Cu^0nanograins from the reduction of Cu^{2+} by Li during cycling results in capacity fade, but after cycling over a long period, they may become active and participate in reactions that enhance the electrochemical reactivity. By offering high Li^+ diffusion coefficients and a large amount of contact surface area between the electrode and electrolyte, the copper can quickly absorb and store vast numbers of lithium ions without causing any deterioration in the electrode.[49] The second reason may due to the electrochemical milling effects, which changes the morphology and decrease the size of the metal particles as well.[48, 50] The results reported are consistent with the second reason and are well supported by the electrode SEM images of before and after 600 cycles at 1000 mA g^{-1} current rate. (Fig. S11 (ESI†)). Such structural change is well understood to improve and boost the reaction with lithium material.

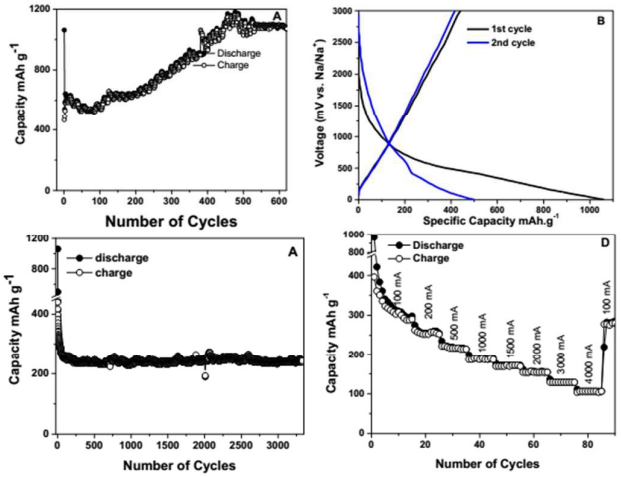

Figure 3. Lithium-ion-battery performance: A) Cyclability test of Cu_{ox}-rGO composite electrode at a current density of 1000 mA g^{-1}; **Sodium-ion-battery performance**: B) Discharge/charge curves of the Cu_{ox}-rGO composite electrode at a current density of 500 mA g^{-1}, C) Cycling performance of the Cu_{ox}-rGO composite electrode at a current density of 500 mA g^{-1}, D) Rate capacity of Cu_{ox}-rGO composite electrode.

Fig. 3B shows the electrochemical performance of Cu_{ox}-rGO was investigated using Na half cells in the range of 0.005−3.0 V. It displays typical charg-discharge curves of Cu_{ox}-rGO at a current density of 500 mA g^{-1}. In the first cycle, it deliver the discharge and charge capacities of 1060 and 439 mAh g^{-1}, respectively, showing a Coulombic efficiency of ~41.41%. This is caused by the side reactions of electrolyte and the formation of SEI. For the evaluation of the long-term cycle stability of the Cu_{ox}-rGO electrode, the electrode was galvanostatically discharged and charged at 500 mA g^{-1} for 3400 cycles (Figure 3C). There was practically no capacity decrease was observed. The superior cycle stability of the Cu_{ox}-rGO electrode for reversible Na^+ storage was highly repeatable. Fig. 3D shows the rate capability of Cu_{ox}-rGO 100 to 4000 mA g^{-1}. The test began with the current density of 100 mA g^{-1}, where the discharge

capacity was consistently ~290 mAh g^{-1} for the first ten cycles. When the current density was increased in steps to 200, 500, 1000, 1500, 2000, 3000 and 4000 mA g^{-1}, the capacity decrease was very small for a battery material. The discharged capacities were retained when the current density was returned to 100 mA g^{-1}. The negligible changes in discharge capacity with current density changes indicate the resilience of the Cu_{ox}-rGO hybrid structure. Evidently the large interlayer spacing allowed Na^+ transport to be carried out at high rates (high current densities) without causing irreversible changes to the hybrid structure.

In summary, we successfully prepared Cu_{ox}-rGO composite by the use of MOFs as the precursors along with metal oxide and graphene oxide as the backbone through a facile two-step annealing process. As a proof of concept, the obtained Cu_{ox}-rGO composite was used in lithium-ion and sodium-ion battery.

Acknowledgements

This work is supported by National Science Council, Taiwan (Project no. NSC 102-2811-M-003-005 and NSC 103-2811-M-003-002). Authors are also grateful to Dr. Di-Yan Wang, Dr. Tsung-RongKuo and Vipin Kumar for their helpful discussion.

References

1 T. Kazda, J. Vondrák, V. Di Noto, M. Sedlaříková, P Čudek, L. Omelka, L. Šafaříková and V. Kašpárek, *J Solid State*Electrochem, 2015, **19**, 1579.
2 G, Pagot, F. Bertasi, G. Nawn, E. Negro, G. Carraro, D. Barreca, C. Maccato , S. Polizzi , and V. Di Noto, *Adv. Funct. Mater.,* 2015, **25**, 4032.
3 P. Poizot, S. Laruelle, S. Grugeon, L. Dupont and J-M. Tarascon, *Nature,* 2000, **407**, 496.
4 J. Cabana, L. Monconduit, D. Larcher and M. R. Palacin, *Adv. Mater.,* 2010, **22**, E170.
5 M. V. Reddy, G. V. Subba Rao and B. V. R. Chowdari, *Chem. Rev.,* 2013, **113**, 5364.
6 O. M. Yaghi, G. M. Li and H. L. Li, *Nature,* 1995, **378**, 703.
7 R. Kitaura, S. Kitagawa, Y. Kubota, T. C. Kobayashi, K. Kindo, Y. Mita, A. Matsuo, M. Kobayashi, H. C. Chang, T. C. Ozawa, M. Suzuki, M. Sakata and M. Takata, *Science*, 2002, **298**, 2358.
8 H. K. Chae, D. Y. Siberio-Perez, J. Kim, Y. Go, M. Eddaoudi, A. J. Matzger, M. O'Keeffe, O. M. Yaghi, *Nature*, 2004, **427**, 523.
9 S. Hasegawa, S. Horike, R. Matsuda, S. Furukawa, K. Mochizuki, Y. Kinoshita and S. Kitagawa, *J. Am. Chem. Soc.,* 2007, **129**, 2607.
10 M. Dinca and J. R. Long, *Angew. Chem., Int. Ed.,* 2008, **47**, 6766.
11 S. Stankovich, D. A. Dikin, G. H. B. Dommett, K. M. Kohlhaas, E. J. Zimney, E. A. Stach, R. D. Piner, S. B. T. Nguyen and R. S. Ruoff, *Nature,* 2006, **442**, 282.
12 D. A. Dikin, S. Stankovich, E. J. Zimney, R. D. Piner, G. H. B. Dommett, G. Evmenenko, S. B. T. Nguyen and R. S. Ruoff, *Nature,* 2007, **448**, 457.
13 B. C. Brodie, *Ann. Chim. Phys*., 1860, **59**, 466.
14 T. Szabo, E. Tombacz, E. Illes and I. Dekany, *Carbon,* 2006, **44**, 537.
15 A. Lerf, H. He, M. Forster and J. Klinowski, *J. Phys. Chem. B,*1998, **102**, 4477.
16 M. D. Stoller, S. J. Park, Y. W. Zhu, J. H. An and R. S. Ruoff, *NanoLett*. 2008, **8,** 3498.
17 W. Shi, J. Zhu, D. H. Sim, Y. Y. Tay, Z. Lu, X. Zhang, Y. Sharma, M. Srinivasan, H. Zhang, H. H. Hng and Q. Yan, *J. Mater. Chem.,* 2011, **21**, 3422.
18 Y. Wang, X. Yang, L. Qiu and D. Li, *Energy Environ. Sci.,* 2013, **6**, 477.
19 C. Peng, B. Jiang, Q. Liu, Z. Guo, Z. Xu, Q. Huang, H. Xu, R. Tai and C. Fan, *Energy Environ. Sci.,* 2011, **4**, 2035.
20 C. Petit and T. J. Bandosz, *Adv. Mater.,* 2009, **21**, 4753.
21 Z.-H. Huang, G. Liu and F. Kang, *ACS Appl. Mater. Interfaces,* 2012, **4**, 4942-4947.
22 J. H. Lee, S. Kang, J. Jaworski, K.-Y. Kwon, M. L. Seo, J. Y. Lee and J. H. Jung, *Chem. Eur. J.,* 2012, **18**, 765.
23 S. Liu, L. Sun, F. Xu, J. Zhang, C. Jiao, F. Li, Z. Li, S. Wang, Z. Wang, X. Jiang, H. Zhou, L. Yang and C. Schick, *Energy Environ. Sci.* 2013, **6**, 818.
24 F. Li, X. Jiang, J. Zhao and S. Zhang, *Nano Energy*, 2015, **16**, 488
25 O. Wee-Jun, T. Lling-Lling, C. Siang-Piao, Y. Siek-Ting and A. R. Mohamed, *Nano Energy*, 2015, **13**, 757.
26 O. Wee-Jun, Y. Jia-Jun, T. Lling-Lling, B. T. Goh, Y. Siek-Ting and C. Siang-Piao, *RSC Adv.,* 2014, **4**, 59676.
27 M. Jahan, Q. Bao and K. P. Loh, *J. Am. Chem. Soc.,* 2012,**134**, 6707.
28 B. Wang, X. L. Wu, C. Y. Shu, Y. G. Guo and C. R. Wang, *J. Mater. Chem.,* 2010, **20**, 10661.
29 L. Q. Lu and Y. Wang, *J. Mater. Chem.,*2011, **21**, 17916.
30 Y. J. Mai, X. L. Wang, J. Y. Xiang, Y. Q. Qiao, D. Zhang, C.D. Gu and J. P. Tu, *Electrochim. Acta,* 2011, **56**, 2306.
31 J. S. Zhou, L. L. Ma, H. H. Song, B. Wu and X. H. Chen, *Electrochem. Commun*. 2011,**13**, 1357.
32 S. Liu, J. Q. Tian, L. Wang, Y. L. Luo and X. P. Sun, *Catal. Sci. Technol.,* 2012, **2**, 339.
33 L. Q. Lu and Y. Wang, *Electrochem. Commun*., 2012, **14**, 82.
34 R. Sahay, P. Suresh Kumar, V. Aravindan, J. Sundaramurthy, W. Chui Ling, S.G. Mhaisalkar, S. Ramakrishna and S. Madhavi, *J. Phys Chem. C,* 2012, **116**, 18087.
35 N. Pereira, L. Dupont, J. M. Tarascon, L. C. Klein and G. G. Amatucci, *J. Electrochem. Soc.,* 2003, **150**, A1273.
36 S. Grugeon, S. Laruelle, R. Herrera-Urbina, L. Dupont, P. Poizot and J.-M. Tarascon, *J. Electrochem. Soc.* 2001, **148**, A285.
37 Z. Da-Wei, Y. Tang-Hong and C. Chun-Hua, *Nanotechnology*, 2005, **16**, 2338.
38 E.J. Cairns and P. Albertus, *Annu. Rev. Chem. Biomol. Eng.* 2010, **1** 299.
39 D. Britt, D. Tranchemontagne and O.M. Yaghi, *Proc. Natl. Acad. Sci. USA* 2008, **105**, 11623.
40 X. Xu, R. Cao, S. Jeong and J. Cho, *Nano Letters* 2012, **12**, 4988.
41 H. Wu, M. Xu, H. Wu, J. Xu, Y. Wang, Z. Peng and G. Zheng, *J. Mater. Chem.,* 2012, **22**, 19821.
42 Y. J. Mai, X. L. Wang, J. Y. Xiang, Y. Q. Qiao, D. Zhang, C. D. Gu and J. P. Tu, *ElectrochimicaActa,* 2011, **56**, 2306.
43 D. J. Lee, J. Choi, M. H. Ryou, C. H. Kim, Y. Min Lee and J. K. Park, *J. Mater. Chem. A*, 2014, **2**, 2906.
44 Y. Wu, M. V. Reddy, B. V. R. Chowdari and S. Ramakrishna, *ACS Appl. Mater. Interfaces,* 2013, **5**, 12175.
45 Y. Liu, V. I. Artyukhov, M. Liu, A. R. Harutyunyan and B. I. Yakobson, *J. Phys. Chem. Lett.,* 2013, **4,** 1737.
46 P. Shaikshavali, K. R. Naresh, M. V. Reddy, V.V. S. S. Srikanth and B. V. R. Chowdari, *ACS Appl. Mater. Interfaces,* 2015, **7**, 2301.
47 J. Chen, L. Xu, W. Li, X. Gou, *Adv. Mater.,* 2005, **17**, 582.
48 Y. Yu, Y. Shi and C. H. Chen, *Nanotechnology,* 2007, **18**, 055706.
49 D. Larcher, C. Masquelier, D. Bonnin, Y. Chabre, V. Masson, J.-B. Leriche and J. M. Tarascon, *J. Electrochem. Soc.,* 2003, **150,** A133.
50 D.W. Zhang, C.H. Chen, J. Zhang and F. Ren, *Chem. Mater*. 2005, **17**, 5242.

